Bioactive Materials 5 (2020) 768–778

Contents lists available at ScienceDirect

Bioactive Materials

journal homepage: http://www.keaipublishing.com/biomat

Biofilm-inspired adhesive and antibacterial hydrogel with tough tissue integration performance for sealing hemostasis and wound healing

Wei Han[a], Bo Zhou[b], Kai Yang[a], Xin Xiong[c], Shifang Luan[d], Yu Wang[a], Zheng Xu[a], Peng Lei[a], Zhengshan Luo[a], Jian Gao[f], Yijing Zhan[a], Guopu Chen[e], Lei Liang[e], Rui Wang[a,*], Sha Li[a,**], Hong Xu[a,***]

[a] State Key Laboratory of Materials-Oriented Chemical Engineering, College of Food Science and Light Industry, Nanjing Tech University, Nanjing, 211816, PR China
[b] Department of Gastrointestinal Surgery, Department of General Surgery, The First Affiliated Hospital of Anhui Medical University, 218 JiXi Avenue, Hefei, 230022, Anhui, PR China
[c] Natural and Medical Sciences Institute at the University of Tübingen, Markwiesenstr. 55, 72770, Reutlingen, Germany
[d] State Key Laboratory of Polymer Physics and Chemistry, Changchun Institute of Applied Chemistry, Chinese Academy of Sciences, Changchun, 130022, PR China
[e] Department of Comparative Medicine, Jinling Hospital, No. 305 Zhongshan East Road, Nanjing, 210002, PR China
[f] School of Marine and Bioengineering, Yancheng Institute of Technology, Yancheng, 224051, PR China

ARTICLE INFO

Keywords:
Biofilm
Mussel
Dual-biomimetic
Adhesive
Hydrogel
Hemostasis
Antibacterial

ABSTRACT

Uncontrolled bleeding and infection can cause significant increases in mortalities. Hydrogel sealants have attracted extensive attention for their ability to control bleeding. However, because interfacial water is a formidable barrier to strong surface bonding, a challenge remains in finding a product that offers robust tissue adhesion combined with anti-infection properties. Inspired by the strong adhesive mechanism of biofilm and mussels, we report a novel dual bionic adhesive hydrogel (DBAH) based on chitosan grafted with methacrylate (CS-MA), dopamine (DA), and N-hydroxymethyl acrylamide (NMA) via a facile radical polymerization process. CS-MA and DA were simultaneously included in the adhesive polymer for imitating the two key adhesive components: polysaccharide intercellular adhesin (PIA) of *staphylococci* biofilm and 3,4-dihydroxy-L-phenylalanine (Dopa) of mussel foot protein, respectively. DBAH presented strong adhesion at 34 kPa even upon three cycles of full immersion in water and was able to withstand up to 168 mm Hg blood pressure, which is significantly higher than the 60–160 mm Hg measured in most clinical settings. Most importantly, these hydrogels presented outstanding hemostatic capability under wet and dynamic in vivo movements while displaying excellent antibacterial properties and biocompatibility. Therefore, DBAH represents a promising class of biomaterials for high-efficiency hemostasis and wound healing.

1. Introduction

Uncontrolled bleeding following trauma or surgery is a major cause of global trauma mortality [1–3]. In particular, bleeding-induced infection is one of the significant cause of complications in tissue regeneration, resulting in inflammatory response and delayed healing in wounds [4,5]. Hydrogel-based hemostatic materials have drawn significant attention in recent years because they act as sealants to control bleeding [1,3,6,7], which provides a barrier against infection by microorganisms [4,8,9] and creates a suitable microenvironment for accelerated wound healing [10,11]. Although existing hemostatic agents based on hydrogels are beneficial, these materials are far from ideal because of their poor tissue adhesion, particularly under wet and dynamic hemorrhage conditions [12,13]. A major barrier to adhesion is interfacial water, which is present as a film on tissue surfaces. Specifically, water molecules in continuous blood flow initiate hydrogen interaction with the functional groups of hydrogels, which significantly weakens the adhesive strength at the interface between the hydrogel and the tissue [14–16]. Catechol chemistry inspired by the wet adhesion of mussels has provided a valuable biomimetic resource for developing diverse adhesive hydrogel for use in aqueous environments [17–19]. However, catechol is easily oxidized with an increase in time,

Peer review under responsibility of KeAi Communications Co., Ltd.
* Corresponding author.
** Corresponding author.
*** Corresponding author.
E-mail addresses: ruiwang2013@njtech.edu.cn (R. Wang), lisha@njtech.edu.cn (S. Li), xuh@njtech.edu.cn (H. Xu).

https://doi.org/10.1016/j.bioactmat.2020.05.008
Received 14 April 2020; Received in revised form 24 May 2020; Accepted 28 May 2020

which leads to gradual weakening of the hydrogel's adhesive strength [20–22].

To address these limitations, primary strategies include the design of hydrogels with the ability to displace the layer of interfacial water at the adhesive interface to facilitate bonding with the tissue [12,13,23,24]. Several adhesive hydrogels with hydrophobic structure have been developed to induce spontaneous coacervation at the contact surface for rapid removal of the interfacial water, resulting in enhanced interaction of adhesive groups with the dry tissue surface [12,13]. Despite such progress, however, one major limitation needs to be addressed: The robust adhesion property of hydrogels can also lead to the adhesion of bacteria in the environment, which results in hydrogels contamination and potentially wound infection. Therefore, the challenge remains to combine the properties of strong adhesion under wet conditions and antibacterial performance in hydrogel hemostatic materials.

Staphylococci have the ability to form sticky biofilm matrices that adhere to wet and dynamic surfaces such as river rocks, deep-sea vents, plant roots in the rhizosphere, and indwelling medical devices in the human body [25,26]. This type of biofilm exhibits impressive adhesive force in the micro Newton range, making it one of the strongest biological adhesives yet described [25,27]. Moreover, a curing mechanism in this biofilm enables the adhesion strength of the holdfast to increase logarithmically with the time of surface contact [28]. Previous studies have shown that the adhesin in staphylococcal biofilm is a gel-like material composed partly of cationic polysaccharides, protein, and DNA [29]. Among these components, cationic polysaccharide intercellular adhesin (PIA) (Scheme 1a) plays a key role in cell−surface adhesion [30,31]. About 20% of the monomers in PIA are deacetylated; the remaining 80% hydrophobic residues (-CH_3) can displace the interfacial water between the bacterium and the surface, thereby promoting close contact between the cationic free amine group ($GlcNH^{3+}$) and the surface [25,31]. Although biofilm is usually considered to be a vexing problem and is difficult to remove, the mechanism of PIA-mediated adhesion has inspired the design of a novel adhesive hydrogel. The adhesive hydrogels driven by PIA molecules are expected to exhibit robust adhesive behavior on the wet and dynamic surface of tissue bleeding uncontrollably.

Herein, we develop a dual biomimetic strategy to prepare adhesive hydrogel (DBAH) driven by staphylococcal biofilm (PIA) and mussel adhesive proteins (Dopa). As depicted in Scheme 1b, the DBAH was fabricated on the basis of a synthetic polymer, CS-MA-*g*-poly(NMA-*co*-DA), consisting of chitosan (CS) grafted with methacrylate (CS-MA), dopamine (DA), and N-hydroxymethyl acrylamide (NMA) via a radical polymerization process. CS-MA is a biomimetic polymer that mimics the structure of PIA with about 80% of the monomers as hydrophobic residues (-CH_3) and 20% as cationic free amine group ($GlcNH^{3+}$). DA is a derivative of L-3,4-dihydroxyphenylalanine (DOPA), which is abundant in mussel adhesive proteins. When DBAH is in contact with water, the abundant hydrophobic residues (-CH_3) aggregates and quickly forms coacervates, thus self-repelling the water molecules on the substrate surface (Scheme 1c). At this point, more catechol groups of DA and cationic free amine groups NH^{3+} of CS-MA are exposed outward, promoting sufficient contact with the adherent substrate to achieve rapid and strong wet tissue integration. This superior tissue integration endows DBAH with excellent hemostasis ability by sealing the bleeding wound even in the wet and dynamic environment of a rabbit's heart (Scheme 1d). In addition, owing to the protective screen of DBAH and the intrinsic antibacterial property of CS, the DBAH scaffold shows good anti-infection capability while maintaining biocompatibility. All of these biomedical functions for DBAH demonstrate its high applicability to wound healing.

2. Experimental

2.1. Materials

The DA, MA, and BIS used in this study were purchased from Shanghai Macklin Biochemical Co., Ltd. (Shanghai, China). The CS, with an average molecular weight of $M_\eta = 3 \times 10^5$ and 70% degree of deacetylation, was obtained from Yangzhou Rixing Bo-Tech Co., Ltd. (Yangzhou, China). The NMA and TEMED were obtained from Shanghai Aladdin Bio-Chem Technology Co., Ltd. (Shanghai, China). Sodium hydroxide (NaOH) with a purity of ≥97.0%, which was used as the ACS reagent; acetic acid; MTT; and APS were acquired from Sigma–Aldrich. The live/dead cell staining kit, phosphate buffered solution (PBS; 0.01 M pH 7.2–7.4), and Dulbecco's Modified Eagle Medium (DMEM) were purchased from Beijing Solarbio Science & Technology Co., Ltd. (Beijing, China). The diamidino-2-phenylindole staining kit was acquired from Nanjing KeyGen Biotech Co., Ltd. (Nanjing, China). The lysogeny broth (LB) medium and agar powder were obtained from Oxid.

2.2. Synthesis and characterization of CS-MA

First, the CS-MA was synthesized as previously reported with some modifications [31]. The acetic acid solution of 1% CS was prepared for use, and MA was then added dropwise to the CS solution to reach molar ratios of 1:3, 1:6, and 1:9 CS/MA, respectively. The mixture was allowed to react at 60 °C for 8 h. The unreacted MA was dialyzed against deionized water for three days. After freeze-drying, the products of CS-MA with different grafting degrees were recorded as CS-MA1, CS-MA2, and CS-MA3. The degree of substitution (DS) of CS-MA was calculated by the ratio of integrated area of the methylene (Ha) peaks at 5.4 ppm and 5.7 ppm to that of the Hb–He peaks at 2.5–4.2 ppm according to Eq. (1).

$$DS = \frac{\text{AH (5.4\&5.7) /2}}{\text{AH (2.5\&4.2) /5}} \times 70\% \quad (1)$$

2.3. Fabrication and characterization of DBAH

The DBAH was synthesized by using the following procedures. (1) CS-MA, DA, NMA, APS, and BIS were mixed in an ice bath under stirring. The compositions of the different hydrogels are listed in Fig. 2a. The mixtures were stirred until a clear solution appeared, followed by adding a few drops of TEA to create basic conditions (pH = 8). After 10 min of mixing, the solution was polymerized at room temperature to form DBAH. Hydrogels with different weight ratios of (CS-MA)/DA were synthesized to investigate the effects of (CS-MA)/DA on the properties of the hydrogels. The time at which the hydrogel did not flow was regarded as the gelation time. Each test was performed in triplicate. (2) The DBAH was soaked in deionized water for 6–8 h and was then immersed in ethyl alcohol (95%) containing about 10% water for 3–5 h; this procedure was repeated three times. Finally, the hydrogel was soaked in ethyl alcohol (95%) for 3 h and was dried in air. The NMA monomer in the hydrogel extract was analyzed by HPLC (Agilent 1260 Infinity II) to determine the purification efficiency. Unless otherwise noted, all of the tests and biological experiment described below used purified DBAH.

2.4. Microstructure

All DBAH samples of swelling equilibrium for SEM analysis were first freeze-dried and were then sprayed with Au film to provide a conductive environment. The morphologies of the hydrogels were observed by SEM (Hitachi TM3000) with a working distance of 20 mm under an accelerating voltage of 15 kV.

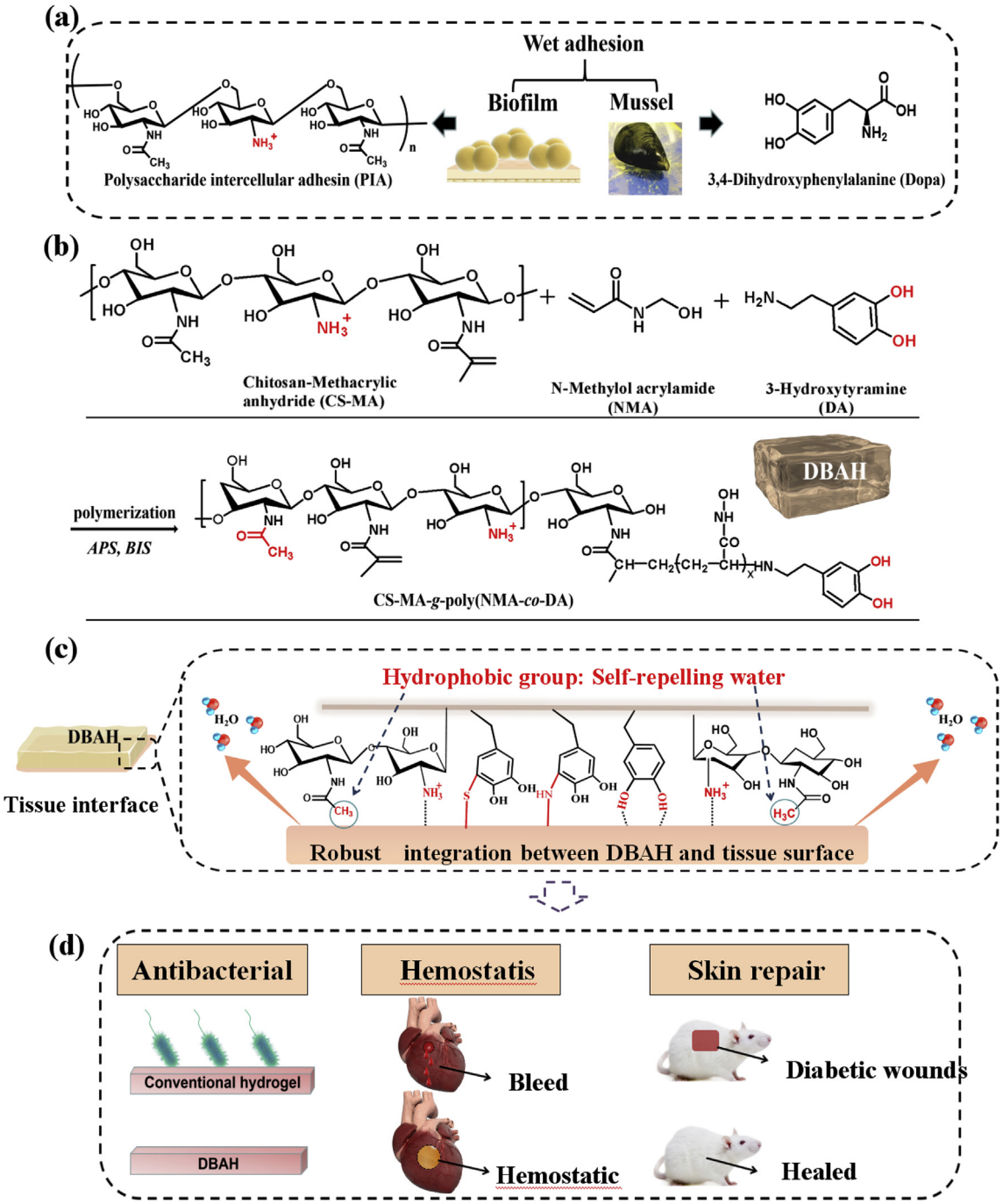

Scheme 1. Schematic illustration of design strategy of an engineered biofilm and mussel inspired dual-bionic adhesive hydrogels (DBAH), and its application for Sealing Hemostasis and Wound Healing. (a) The structure of polysaccharide intercellular adhesin (PIA) derived from biofilm and DOPA derived from mussel protein that play a key role in wet adhesion; (b) A biomimetic biopolymer, chitosan grafted with methacrylate (CS-MA) from PIA, and Dopamine, a catecholamine containing a catechol group of DOPA, was conjugated with NMA for hydrogel formation; (c) Schematic illustration of strong underwater bioinspired adhesion base on the self-repelling water function of CS-MA. (d) The multifunctional properties and potential application in in vivo hemorrhage and diabetic wound healing with antibacterial performance.

2.5. Swelling tests

The initial weight of DBAH was accurately measured after being freeze-dried. Then, the hydrogel samples were immersed in a PBS buffer (pH = 7.4) at 25 ˚C and were swollen until the equilibrium state was reached. After specified time intervals, the swollen hydrogels were weighed after gently removing excess water using filter paper. The swelling ratio is defined as follows:

$$Qt = \frac{Wi - W0}{W0} \quad (2)$$

where W_i and W_0 represent the weights of the swollen and initial samples, respectively.

2.6. Mechanical properties tests

A dynamic mechanical analyzer (MCR102, Anton Paar, Austria) was used to analyze the rheological properties of the DBAH including the

storage modulus (G′) and loss modulus (G″). First, the purified DBAH was prepared according to the above method. All samples were cut into cylindrical shapes 25 mm in diameter × 1 mm in height. The linear viscoelastic region of each hydrogel sample was determined by strain scanning under the conditions of 37 °C and 1 Hz frequency. Under the conditions of 37 °C and 0.1% strain, the variation in G' and G″ at the frequency range of 0.1–100 Hz was studied by using the oscillatory shear deformation mode.

2.7. Wet adhesive properties of DBAH

The wet adhesive strength of the DBAH was measured by performing lap-shear strength tests on porcine skin and were quantitatively analyzed according to a method described in previous research [9]. Fresh porcine skins were obtained from local markets and were kept in a freezer at −4 °C until use. The skins were then cut into sheets of 5 cm × 2 cm, and excess fat was removed. The measurement was performed using a universal test machine (Instron 3340), and the values were calculated by dividing the maximum load by the corresponding overlapping area of each sample. DBAH samples with dimensions of 2.0 cm × 2.0 cm with different DS of CS-MA (DBAH CS-MA1 DBAH CS-MA2, DBAH CS-MA3) were applied to tissue segments, upon which additional segments of tissue were immediately pressed. The samples were then allowed to cure for 10 min at 37 °C under humid conditions. A tensile tester with a 10 kN load cell was used, and the samples were fixed between the two film clamps with the tensile rate set at 5 mm/min. Five samples for each group (n = 5) were used in the adhesion test. A hydrogel copolymer PDA-PNMA free of CS-MA (SBAH) was also used for analysis as a control.

The morphologies of the adhesive interface samples were first extracted and were then fixed with 2.5% glutaraldehyde in a PBS buffer (0.1 M, pH 7.0) for 5 h. Subsequently, the samples were washed three times for 15 min in a phosphate buffer and were then dehydrated by a graded series of ethanol extractions (20%, 40%, 60%, 80%, 90%, and 100%) for 20 min at each step. Prior to the viewing, the cross-section of the samples were mounted and sprayed with an Au coating. Finally, the samples were observed under using SEM (Philips-FEI, Holland).

To provide a dynamic and wet environment, the DBAH on the surface of the porcine skin substrates were bended and distorted. Flowing water was applied to the interface between the hydrogel and the porcine skin substrates. In addition, adhesion-strip cyclic tests were also conducted 10 times on the surface of wrist skin to evaluate the repeatable adhesiveness and skin's sensitization from the hydrogels.

2.8. Burst pressure measurements

The bursting pressure test was performed according to previous methods following the ASTM F2392 standard protocol [36]. A segment of porcine skin tissue with dimensions of 4 cm × 4 cm and 5 mm in thickness was prepared for this measurement. A 1.5 mm circular incision was first made in the center of the tissue and the surface was kept wet. Then, DBAH 10 mm in diameter and 3 mm in thickness was adhered to the puncture site. The skin tissue with hydrogel was fixed to a measurement device linked to a syringe pump filled with PBS solution. The pressure was continually increased by injecting PBS at 2 mL/min. A digital manometer was used to measure the pressure on the adhesive. The value at which the pressure began to decrease was considered to be the peak pressure. The experiment was repeated three times.

2.9. Antibacterial properties of DBAH

A model of a dressing covering skin tissue was used to evaluate the antibacterial activity of DBAH. As previously mentioned, purified DBAH samples with different ratios of (CS-MA)/DA were prepared. Dressings of gauze, PEGDA hydrogel, and SBAH were used as control groups. Sections of porcine skin with dimensions of 3 cm × 3 cm serving as experimental tissue substrates were cut and cleaned to remove excess fat. The sterile dressings were applied to the surface of the porcine skin and were pressed for 1 min to ensure attachment before being incubated in a constant temperature incubator at 37 °C for 12 h. Then, the dressings were removed, and the possible bacterial survivors on the tissue surface were rinsed with sterile water and diluent. They were then added to the LB agar culture medium and were incubated for 24 h. The colonies forming units were counted and photographed.

2.10. In vitro biocompatibility experiment

The cytotoxicity test of DBAH was performed using an MTT and live/dead assay by co-culture of DBAH extract with NIH-3T3 mouse fibroblasts in vitro. First, the extracts were prepared by incubating DBAH in a DMEM medium at an extraction ratio of 20 mg/ml for 24 h at 37 °C. After the extract was sterilized by 0.22 μm filters and supplemented with 10% fetal bovine serum (FBS). The NIH-3T3 mouse fibroblast (cell concentration = 1×10^4 cells mL^{-1}) was inoculated in a 96-well cell culture plate containing DMEM complete medium at 37 °C overnight. Subsequently, the culture media were removed, and 100 μL of the hydrogel extract was added to the culture plates. The cell proliferation rate was quantified using the MTT assay at 24 h, 48 h, and 72 h, respectively. Additionally, cells were stained using red opaque/ethidium bromide (RO/EB) fluorescent stains and were observed using a fluorescence microscope (Olympus ix73).

2.11. Hemostasis experiments on mouse liver and rabbit heart

The hemostatic ability of DBAH in vivo was first studied by a using a mouse liver hemorrhage models (male Sprague–Dawley rats, 200–220 g, Jinling Hospital, Nanjing, China). All trial protocols and animal handling were conducted in accordance with the Jinling Hospital Animal Survey Ethics Committee. First, the mice were anesthetized with ketamine at 80 mg/kg body weight. Pre-weighed filter paper was placed beneath the liver, and bleeding was induced using a 20 gauge needle. DBAH segments with dimensions of 10 mm × 10 mm × 2 mm were immediately applied to the surface of the bleeding area. The bleeding volume was observed every 30 s, and the total amount of the blood loss was recorded by weighing the papers after 120 s. The hemostatic times were measured for the PU- and PEGDA-treated groups and that with no treatment as controls. The test was repeated three times (n = 3) to obtain the average blood loss.

To further evaluate the hemostatic potential of DBAH in dynamic injuries, hemorrhaging heart models of rats (male Sprague-Dawley rats, 200–220 g, Jinling Hospital, Nanjing, China) and rabbits (New Zealand white, two–four months old) were employed in vivo. After applying general anesthesia, a 20 gauge needle was used to pierce the hearts (n = 5). Then, the defects were rapidly covered with DBAH (10 mm × 10 mm × 2 mm). Photographs and videos were recorded to examine the adhesion and hemostasis activity at different times for a total duration of 5 min. Then, the hydrogels were peeled from the surface of the rabbit heart while images were recorded.

2.12. Wound healing study

All animal handling and protocols were approved by the Animal Ethics Committee of Jinling hospital, Nanjing, China. A mouse model of an infected full-thickness cutaneous wound was used to evaluate the effects of DBAH on wound healing. First, 24 healthy male Sprague-Dawley rats (180–250 g) received general anesthesia. Their backs were then shaved, and they were randomly divided into four groups. A rounded full-thickness cutaneous excision (1 cm × 1 cm) was performed on each rat, after which 100 μL of a solution containing *S. aureus* (1×10^7 CFU mL^{-1}) was applied to the defects. Subsequently, the four groups were treated with sterilized DBAH, PEG-DA hydrogel, PU wound dressing, and PBS, respectively. The mice were maintained

in separated compartments, and the wounds were allowed to heal for nine days. The wounds were observed, and optical images were taken to record the microscopic self-healing process on days 0, 3, 5, and 7. ImageJ software was used to measure and calculate the wound area to obtain macroscopic wound healing data. The skin explants were collected on day 9, fixed in 10% formalin, and embedded in paraffin. The granulation tissue samples were stained following routine protocols for staining with hematoxylin and eosin (H&E) and Masson's trichrome, and IL-6 was used for immunohistochemistry staining. For neovascularization evaluation, the sections were probed with a primary antibody against CD31 (KEYGEN, KGYM0118–7) and α-smooth muscle actin (α-SMA; KEYGEN, KGYT5053-6). After primary antibody incubation, the skin sections were washed and incubated with FITC-(KEYGEN, KGAA26) and TRITC-(KEYGEN, KGAA98) conjugated secondary antibodies. The nuclei were counterstained with 4, 6-diamidino-2-phenylindole (DAPI).

3. Results and discussion

3.1. Synthesis and characterization of chitosan grafted with methacrylate (CS-MA)

To mimic the structure of PIA, CS-MA was synthesized by specifically conjugating MA groups to amino groups of CS (Fig. 1a), following previous research [31,32] with several modifications. A representative spectrum of ^{1}H NMR analysis of the purified CS-MA polymer is depicted in Fig. 1b. The chemical shifts at 5.4 ppm and 5.7 ppm (a, 2H, CH_2) were assigned to vinyl protons, which are characteristic signals of MA, indicating the successful conjugation of MA to CS. The four peaks at 2.5–4.2 ppm (b, c, d, e; 5H, CH–CH–CH–CH_2) are ascribed to the N-acetylglucosamine ring protons from CS, and the peak at about 1.98 ppm (h, 3H, CH_3) is attributed to the methyl protons of CS. The ratio of MA monomer to N-acetylglucosamine monomer in CS was confirmed by calculating the ratios of vinyl protons (a) and N-acetylglucosamine ring proton (b, c, d, e) groups present in the CS polymer. As shown in Fig. 1c, when the feeding ratios of MA and CS were 1:1, 1:6, and 1:9, the degrees of substitution (DS) of MA were 24%, 36%, and 44%, respectively. Because the deacetylated degree of CS used in this study was 70%, the hydrophobic residues (-CH_3) in the CS backbone were 54%, 66%, and 74%, corresponding to 46%, 34%, and 26% cationic free amine groups ($GlcNH^{3+}$) for CS-MA1, CS-MA2, and CS-MA3. Thus, the obtained CS-MA3 was the biomimetic polymer that are highly consistent with the composition, structure of natural PIA, which contains about 20% deacetylated monomers and 80% cationic free amine groups ($GlcNH^{3+}$). The DS was positively correlated to the ratio of MA used in acylation reaction, which could be accurately controlled by adjusting the ratio of anhydride to amino groups. The DS of CS-MA was 24%, 36%, 44% and 44.2% corresponding to the anhydride to amino groups' molar feed ratios of 3, 6, 9 and 12, respectively. When the feeding ratio of MA and CS was more than 1:9, the DS of the MA no longer increased (Fig. 1b and c), mainly because of the limited solubility of MA.

3.2. Preparation and characterization of dual biomimetic adhesive hydrogel (DBAH)

The DBAH was synthesized on the basis of free radical polymerization reactions of multi-vinyl monomers from CS-MA, DA, and NMA (Fig. 1d). To study the effects of the (CS-MA)/DA weight ratios, the gelation of DBAH in the presence of constant concentrations of NMA, CS-MA3, N, N′-methylenebisacrylamide (BIS), and ammonium persulfate/N, N, N, N-tetramethylethylenediamine (APS/TEMED) was studied. The detailed data are listed in Fig. 2a. The curing behavior of the hydrogel was examined via the inverted vial method (Fig. 2b). Transparent, viscous hydrogel formed when the weight ratio of the (CS-MA3)/DA was 24 wt% and remained stable until it decreased to 3 wt%. This decrease in weight ratio led to an increase in gelation time from 47 s to 74 s (Fig. 2c) because of the gradual reduction in the cross-linking density of the hydrogels. It should be noted that the hydrogel was unable to form when the weight ratio of the (CS-MA3)/DA was less than 1.5 wt%. This phenomenon occurred because the excess reductive DA molecules affected the activity of the initiator (APS) and thus retarded the polymerization of the vinyl monomers.

To prevent the potential cytotoxicity of unreacted NMA monomers,

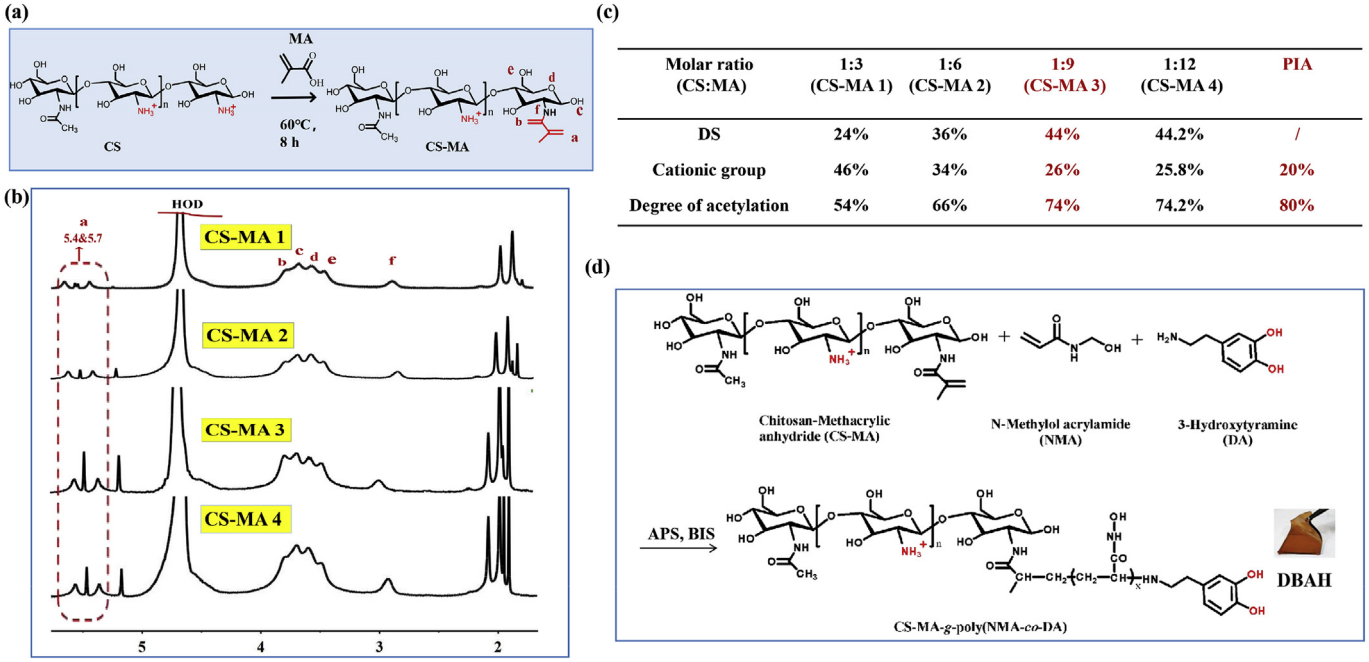

Molar ratio (CS:MA)	1:3 (CS-MA 1)	1:6 (CS-MA 2)	1:9 (CS-MA 3)	1:12 (CS-MA 4)	PIA
DS	24%	36%	44%	44.2%	/
Cationic group	46%	34%	26%	25.8%	20%
Degree of acetylation	54%	66%	74%	74.2%	80%

Fig. 1. Synthesis and structure characterization of CS-MA. (a) Schematic illustration of the synthesis of CS-MA; (b) The ^{1}H NMR spectra of CS-MA with different grafting density of MA (CS-MA1, CS-MA2, CS-MA3, CS-MA4); (c) Synthesis of CS-MA with different degrees of substitution (DS) of MA: CS-MA3 with 26% of the monomers are deacetylated, which is comparable to PIA. (d) The formation of DBAH via free radical polymerization reaction based on CS-MA, DA, and NMA.

(a)

Hydrogels	(CS-MA 3)/DA (wt. %)	NMA (g)	APS/AM (wt. %)	BIS/AM (wt. ‰)	TMEDA (μl)	Water (wt. %)
DBAH 1	24	2	1.5	1	15	100
DBAH 2	12	2	1.5	1	15	100
DBAH 3	6	2	1.5	1	15	100
DBAH 4	3	2	1.5	1	15	100
DBAH 5	1.5	2	1.5	1	15	100

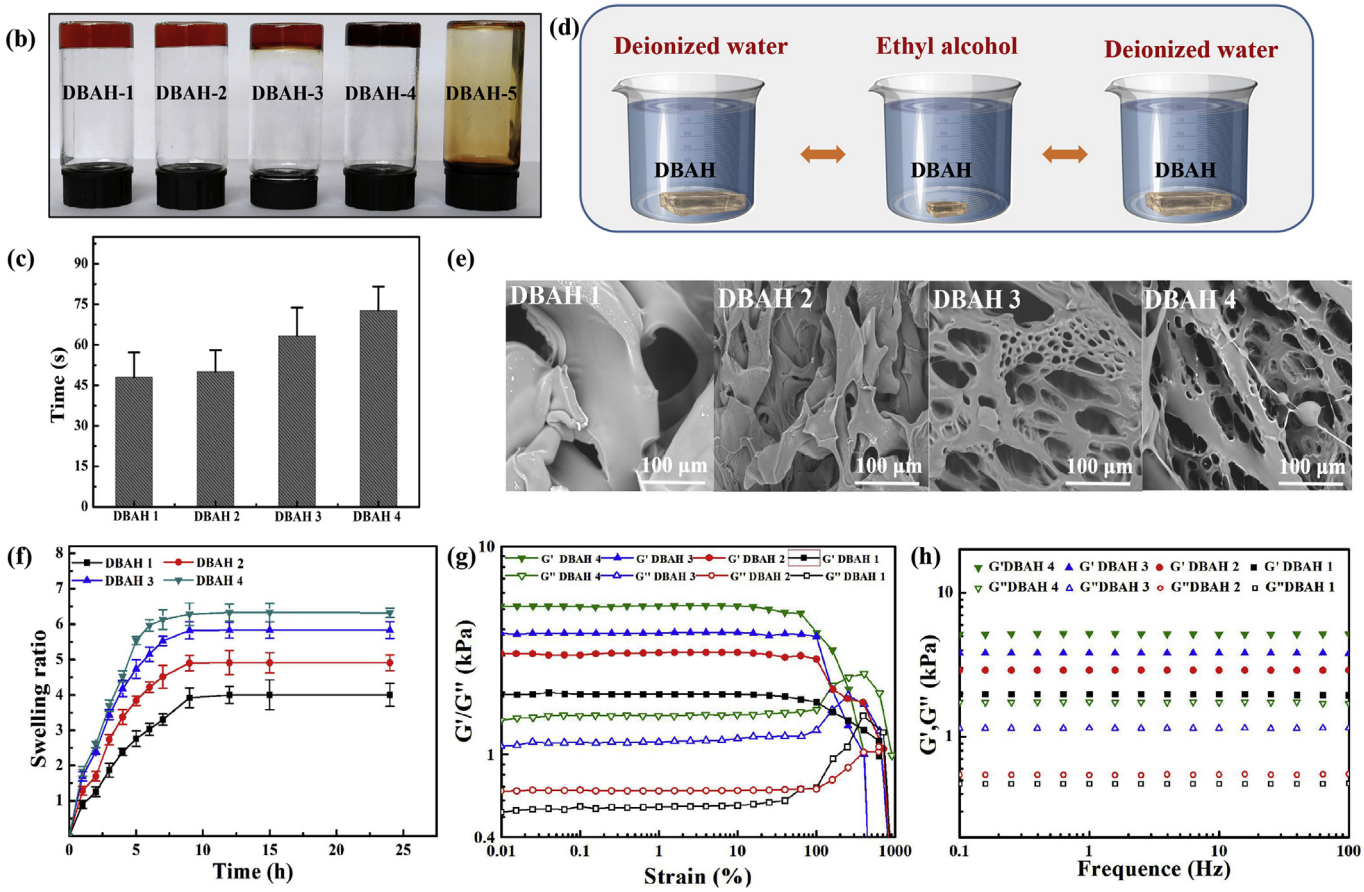

Fig. 2. Physical and mechanical characterization of DBAH. (a) Synthesis of DBAH with different ratio of (CS-MA 3)/DA (wt.%). (b) Hydrogel formation of DBAH with different (CS-MA)/DA (wt. %) (DBAH1: (CS-MA)/DA = 24%, DBAH2: (CS-MA)/DA = 12%, DBAH3: (CS-MA)/DA = 6%, DBAH4: (CS-MA)/DA = 3%). Suitable (CS-MA)/DA (wt. %) ((CS-MA)/DA ≥ 3 wt%) resulted in solid hydrogels. Lower CS-MA contents ((CS-MA)/DA = 1.5 wt%) resulted in viscous solution; (c) Gelation time of different hydrogels; (d) Purification of hydrogels with a three cycles of deionized water and ethanol. (e) Morphologies, (f) Swelling ratio, and (g), (h) Rheological analysis of DBAH.

the DBAH was purified prior to further measurements by repetitive circulation with deionized water and ethyl alcohol (Fig. 2d). The results of high performance liquid chromatography (HPLC) demonstrated that nearly no residual NMA monomers remained in the DBAH after three cycles of purification (Supplementary Fig. S1). Considering previous studies in which most of the acrylamide (AM)-based hydrogels did not remove unreactive AM monomers prior to application, the DBAH in this study showed better biocompatibility. Furthermore, it is widely accepted that the mechanical properties and adhesiveness of AM-based hydrogels weaken significantly when used in aqueous environments. Thus, advance purification is crucial for fabricating hydrogel hemostatic materials in potential clinical applications. Accordingly, all of the DBAH samples used in the present study were purified as described above.

The microstructures of the lyophilized hydrogels were observed by scanning electron microscopy (SEM). Fig. 2e shows that the DBAH displayed a smooth surface with no porous structures when the weight ratios of the (CS-MA3)/DA were 24 wt% and 12 wt%. This result is attributed to the inhomogeneous network formed by rapid cross-linking, which is consistent with the gelation time. With a decrease in the weight ratio of the (CS-MA3)/DA from 12 wt% to 6 wt%, the hydrogels showed interconnected porous structures and microfibril structures owing to the gradual polymerization reaction and the homogeneous cross-linking density of the hydrogels. The best regular pore spacing was observed for the DBAH4 when the (CS-MA3)/DA was at 3 wt%. Fig. 2f also shows that the DBAH4 exhibited more distinct swelling behavior than that in the other groups because the additional porous structures are able to maintain more moisture [33], which is a more suitable characteristic for a hemostatic dressing. The rheological measurements further demonstrated the effect of the weight ratios of (CS-MA)/DA on the mechanical property of DBAH. For all hydrogels, the storage modulus (G′) was consistently higher than the loss modulus (G″), and they exhibited a plateau in the whole frequency range (Fig. 2g and h). This is typical behavior of polymer hydrogels. In addition, with a decrease in the weight ratio of (CS-MA3)/DA from 24 wt% to 3 wt%, the storage modulus of the four DBAHs gradually increased from 2640 Pa to 5047 Pa owing to the more homogeneous and stable network structure compared to SBAH (Fig. S2). These results are consistent

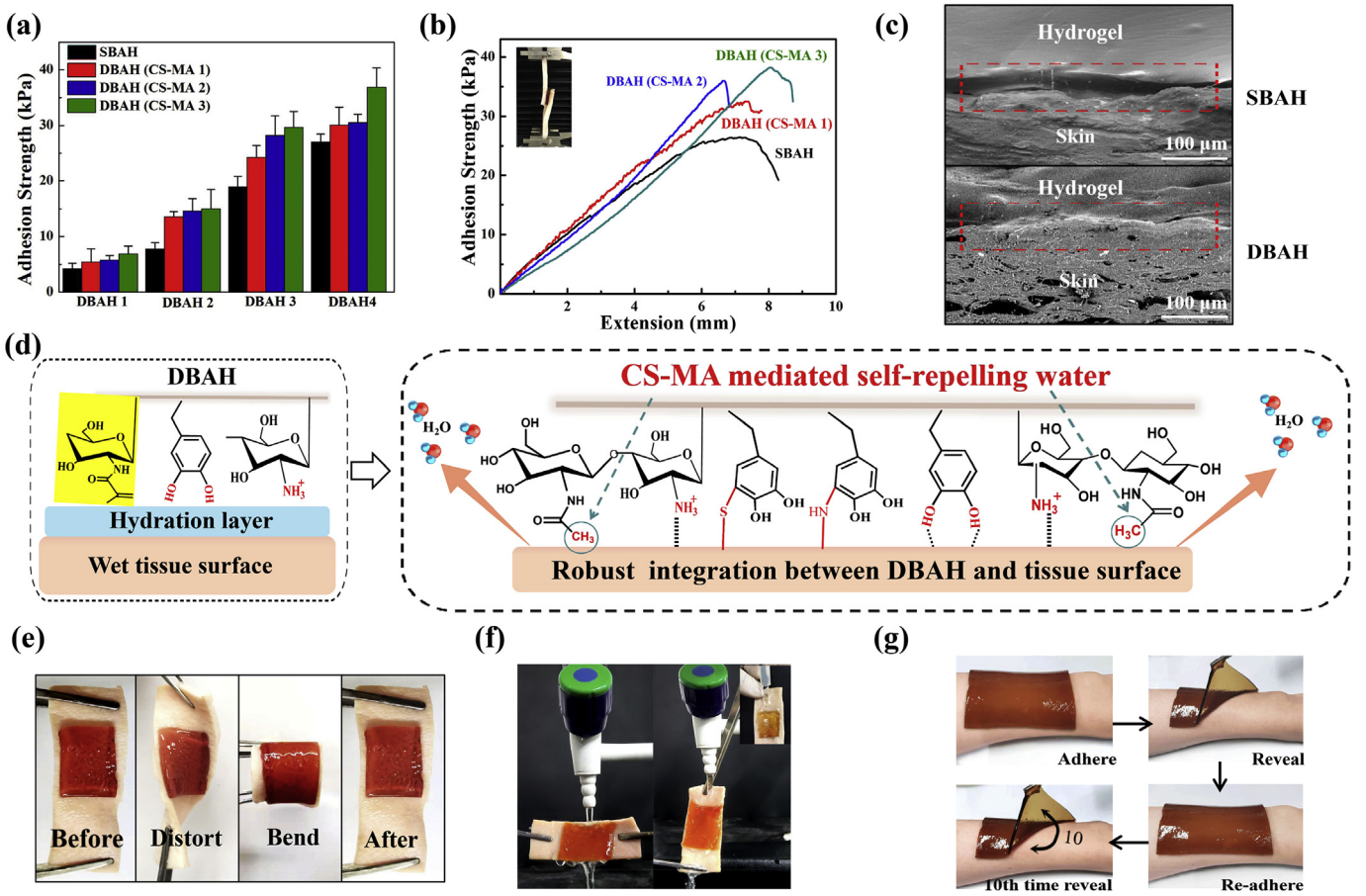

Fig. 3. (a) Adhesive strengths and (b) Lap shear curve of DBAH containing different kind of CS-MA on two pieces of porcine skin. The single biomimetic PDA-PAM hydrogel free of CS-MA as control; (c) Scanning electron micrographs of the interface between the hydrogel and the porcine skin; (d) Schematic illustration showing a potential mechanism of the tissue adhesion of DBAH. (e, f) Photographs of the DBAH adhering to the tissue. No detachment was observed between the hydrogel and tissue regardless of bending, distorting, and even under water flushing. (g) Photos of the multiple times repeatable adhering–peeling process of DBAH on the author's arm while no irritability.

with the hydrogel micromorphology.

3.3. Adhesive behavior of hydrogels

We next evaluated the effect of CS-MA on the adhesion strength of DBAH by comparison with that of single biomimetic adhesive hydrogels (SBAH), the PDA-NMA hydrogels free of CS-MA. As indicated in Fig. 3a and b, the adhesion strength of the DBAH increased with an increase in the DS of the MA; the maximum value of 34 kPa was shown for DBAH4 (CS-MA3). As CS-MA with higher grafting degree has more hydrophobic residues (-CH_3) aggregates and quickly forms coacervates than other CS-MA, thus self-repelling the water molecules on the substrate surface and helping the DBAH anchoring. In addition, There are no hydrophobic residues (-CH_3) aggregates in SBAH, so all of the DBAH samples exhibited much higher adhesion strength than that of the SBAH samples. The ultrastructural appearance of the adhesive interface was further observed by SEM analysis. As shown in Fig. 3c, compared with that of SBAH, a more tightly contacted and seamless interface was observed between DBAH4 (CS-MA3) and the interface tissue, indicating excellent tissue adhesion and integration. This is attributed to the biomimetic design of DBAH inspired by the PIA of biofilm. The proposed mechanism is that when DBAH is in contact with water on the surface of wet tissue, the hydrophobic residues (-CH_3) of CS-MA3 aggregate to rapidly form coacervates, followed by self-removal of the interfacial water and dislodging of the hydration-layer barriers (Fig. 3d). Simultaneously, more catechol groups of DA and cationic free amine groups of CS-MA are exposed outward, accelerating sufficient contact with the wet adherent substrate and achieving robust wet adhesion. The interaction of interfacial forces is based on the binding affinity of DBAH with diverse nucleophiles (e.g., amines, thiol, and carboxyl) of biological molecules on tissue surfaces.

Further, DBAH4 (CS-MA3) remained intact and tightly adhered to the tissue with no detachment through the processes of bending, distortion, and strongly turbulent water flushing (Fig. 3e and f). Moreover, the hydrogel had repeated superior adhesiveness even after 10 cycles of adhesion, and the user has no obvious skin allergywithin 24 h (Fig. 3g). All of these results demonstrate that DBAH is a hemostasis material with strong potential for application for in vivo wet and dynamic environments.

3.4. Burst pressure test

To simulate an in vivo artery hemostasis environment, we utilized burst pressure tests to investigate the capacity of DBAH to withstand blood pressure (Fig. 4a and b). The burst pressure, which was dependent on the CS-MA, was significantly higher for all of the DBAH4 samples (CS-MA1, CS-MA2, CS-MA3) than that for the SBAH samples (Fig. 4c). The highest measurement, 168 mm Hg, was obtained for DBAH4 (CS-MA3), indicating the highest adhesion strength. This result is consistent with the in vitro evaluation of the adhesive strength. The burst pressure of the DBAH4 (CS-MA3) was significantly higher than in most clinical settings (systolic BP 60–160 mm Hg) and exceeded that of commercially available surgical sealants [23,34]. This feature also suggests the potential of DBAH as a sealing agent for hemostasis.

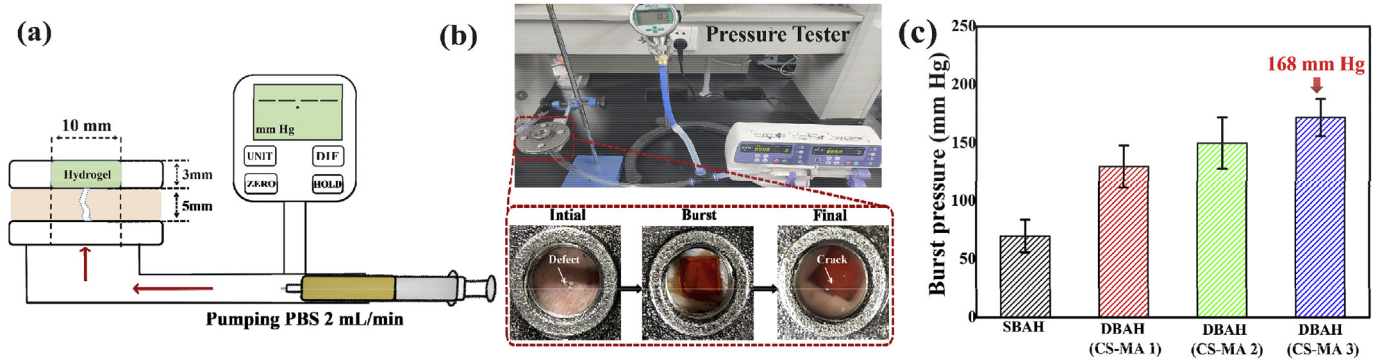

Fig. 4. Burst pressure of DBAH. (a) Schematic diagram; (b) Experimental setup and specimen dimensions for the burst pressure measurement. PBS was pumped into the specimen chamber under a constant flow rate of 2 mL/min, while the pressure was recorded with a pressure gauge; (c) The observed burst pressure of DBAH containing different kind of CS-MA and SBAH.

3.5. Antibacterial performance

The DBAH also showed exceptional antibacterial performance against cell attachment, as determined by applying the hydrogel directly onto the wet surface of porcine skin. As shown in Fig. 5a, after 24 h of cultivation in the presence of bacteria, very few bacteria adhered to the interface of the DBAH and tissue. This result suggests that a tight contact and seamless interface were present between the hydrogel and the covered tissue. In contrast, the weak tissue adhesion and integration of tissue treated with polyurethane (PU) dressing and polyethylene (glycol) diacrylate (PEGDA) hydrogel enabled the invasion of substantially more bacteria. Fig. 5b and c shows that the antibacterial ability also depended on the CS-MA. The best antibacterial effect was shown by DBAH with CS-MA3, which agrees with the adhesion study. Moreover, this feature endows the DBAH with the pivotal capacity to prevent wound infections from impeding the skin repair process.

3.6. In vitro biocompatibility of DBAH

To prove the applicability of DBAH for biomedical applications, the in vitro biocompatibility was investigated against NIH-3T3 mouse fibroblasts. As presented in Fig. 6a, fluorescent confocal microscopy images after live/dead staining showed that the cultured cells were increasingly spindle-shaped and were spread quite well for DBAH between 24 h and 72 h of culture. No significant difference was observed among the DBAH and control group results. The results of 3-(4,5-dimethylthiazol-2-yl)-2,5-diphenyltetrazolium bromide (MTT) assay showed that the optical density (OD) values increased with time and that the cell viability of the DBAH was maintained as high as 87.6% ± 3.2% compared with the control group results after co-culturing for 72 h (Fig. 6b). The results demonstrate that DBAH is relatively nontoxic even at higher polymer concentrations, which is vital for its further application in vivo. This biocompatibility is attributed mainly to the purification process of DBAH prior to application.

3.7. In vivo hemostatic ability of DBAH

The hemostatic ability of DBAH was first evaluated by using mouse liver hemorrhage models (Fig. 7a). Here, to probe the wet adhesive ability of hydrogel for enhancing the hemostatic efficacy, the PEGDA hydrogel, with the significantly weakened adhesive property, was chosen as the positive control. Notably, the bleeding in the liver wound was rapidly controlled within 30 s after treatment with the DBAH dressing. In comparison, that treated with PEGDA hydrogel still displayed obvious bleeding after 120 s (Fig. 7b). In addition, the DBAH-treated liver had significantly less blood loss, at 31.9 ± 5.3 mg,

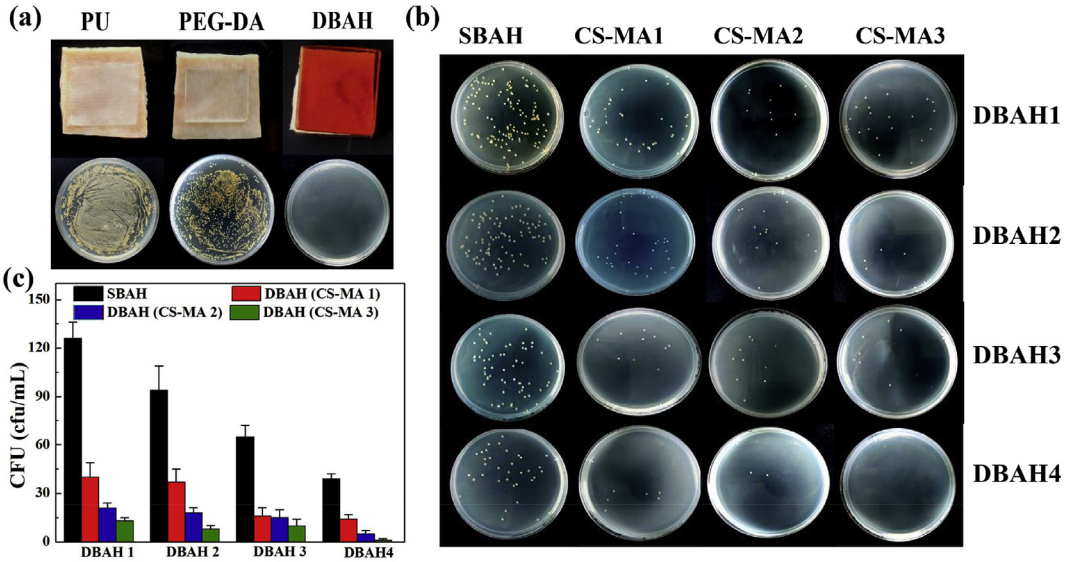

Fig. 5. Antibacterial activity analysis of DBAH. (a) Photos of bacteria clones at the interface of pigskin coverd 12 h with PU dressing, PEG-DA hydrogel and DBAH, respectively; (b) Macroscopical images of bacteria clones and (c) Quantitative bacerial viability of specimen treated by DBAH containing different kind of CS-MA and SBAH.

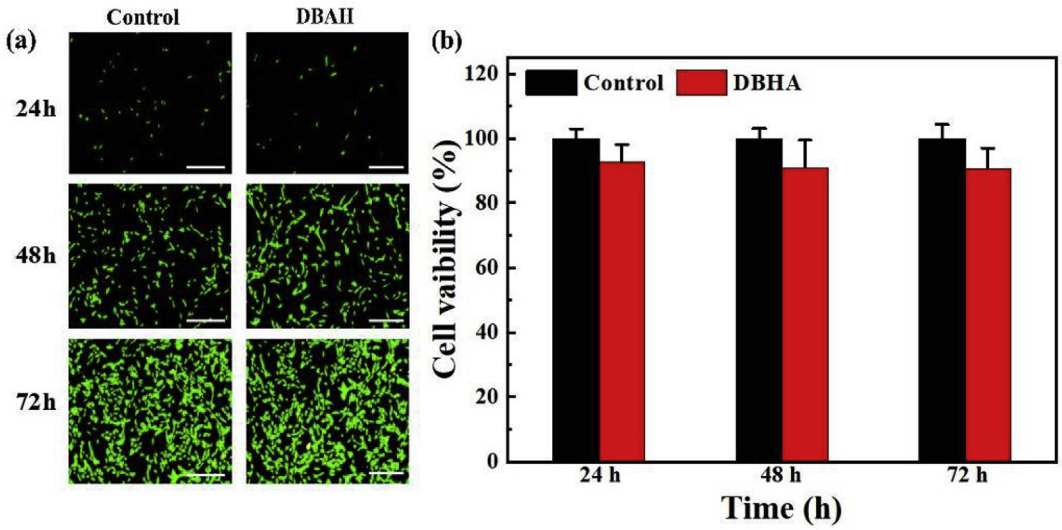

Fig. 6. In vitro cell compatibility. (a) CLSM images of the cells stained with the LIVE/DEAD assay kit after 24, 48 and 72-hour culture on DBAH's extract media. A normal culture medium was used as the control.(b) Cell viability of NIH-3T3 cells after 24, 48, and 72-hour culture in mediums that were conditioned with DBAH. Scale bars = 100 μm.

compared with that in the untreated liver and the liver treated with PEGDA, at 266.1 ± 41.2 mg and 116.5 ± 17.2 mg, respectively, after 120 s (Fig. 7c). The rapid hemostasis ability of DBAH can be attributed to its excellent wet adhesive performance. The mechanism of this material's wet adhesive property, specifically is rapid water repelling ability, is the cross-linked adhesion of the synergistic chemical bonds between the CS-MA and DA at the interface of the liver. The hydrophobic residues (-CH_3) of CS-MA initially dislodges the hydrated bleeding surface and facilitates the subsequent robust binding of CS and DA to the wet liver substrates. At the hemorrhaging site, this material

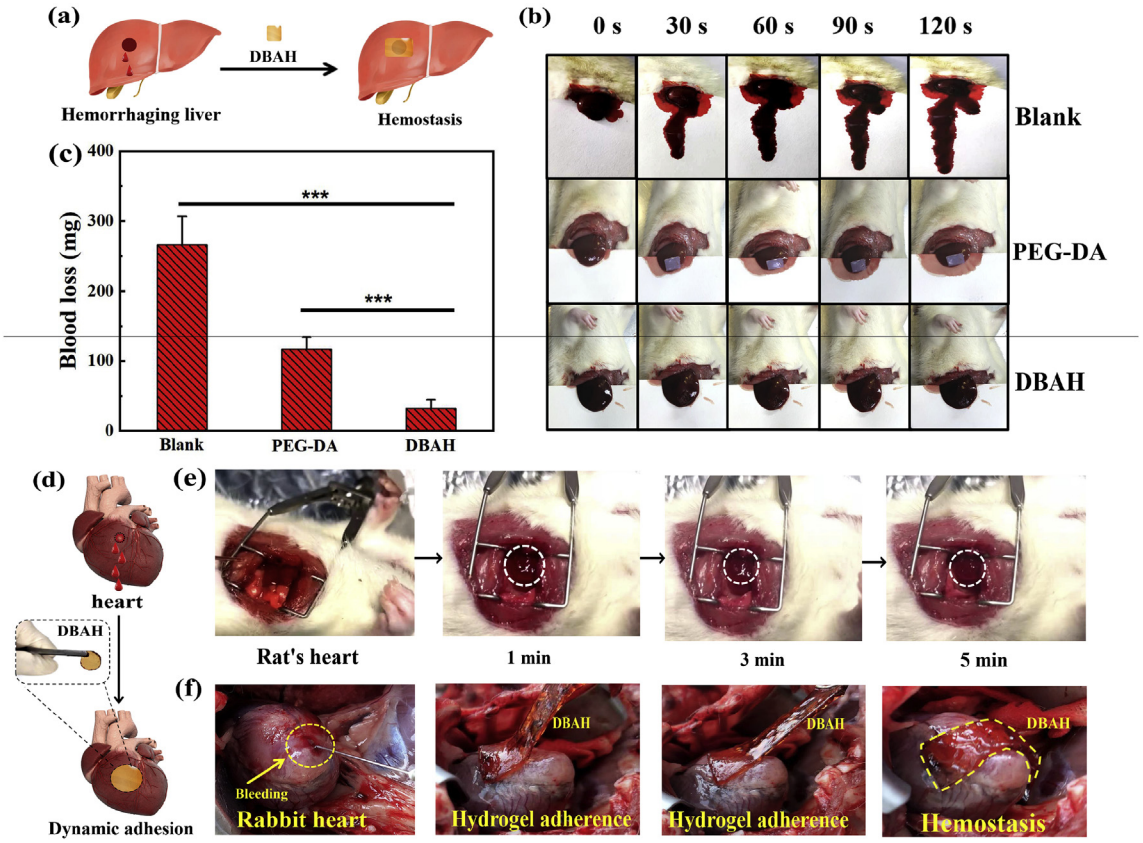

Fig. 7. Hemostatic performance of the DBAH. (a) A schematic illustration of the mouse liver hemorrhage model treated by DBAH; (b) Pictures showing hemostatic efficacy of the damaged SD rats liver treated by DBAH, PEGDA hydrogel (positive control), and untreated (negative control) within 120 s; (c) The accumulated blood loss from liver bleeding treated with different dressing as mentioned above at 120 s ("***" means $p < 0.001$); (d) A schematic illustration of the rabbit's heart bleeding model treated by DBAH; (e) In vivo test on a beating SD rats heart with blood exposure within 5 min; (f) In vivo test on a beating rabbit's heart with blood exposure within 5 min.

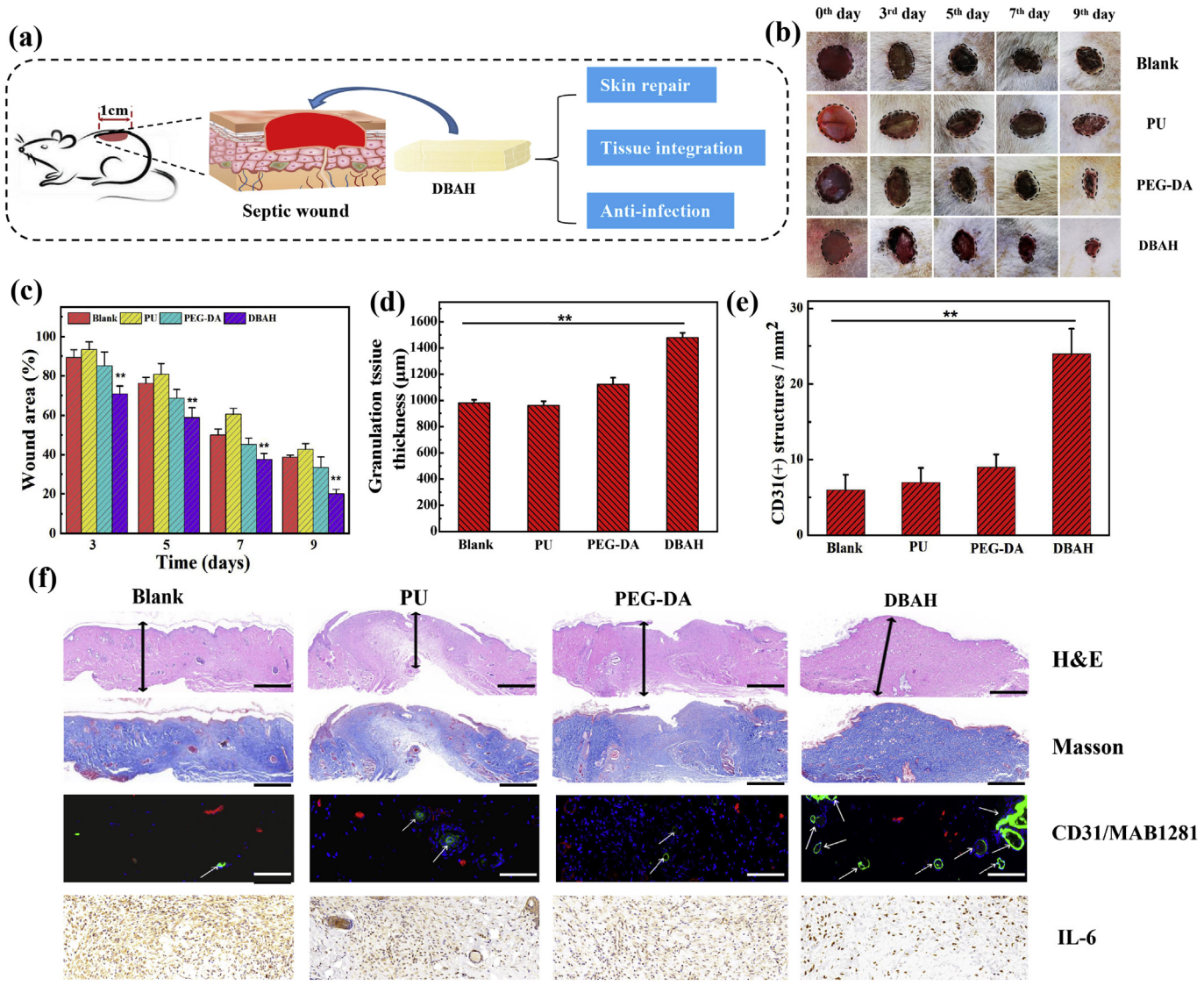

Fig. 8. Evaluation of DBAH in vivo skin repair promotion at wound of SD rat dorsal skin. (a) Schematic illustrations of wound healing process; (b) Photographs of wounds treated with DBAH, PEGDA hydrogel and PU dressing (positive control), and untreated (Blank, negative control) at 0th, 3rd, 5th, 7th and 9th day; (c) Mean wound area and (d) Quantitative analysis of granulation tissue thickness of wounds at 9th day; (e) Quantification of CD31 labeled structures; (f) Hematoxylin–eosin and Masson staining, immunofluorescence staining of neovascularization, and immunostaining of IL-6 in granulation tissues of wounds at 9th day. Scale bars: H&E, Masson = 1 mm, CD31/MAB1281, IL-6 = 100 μm.

forms a hydrogel network barrier in the bleeding liver tissue. An additional pivotal factor is the inherent hemostatic effect of CS.

The in vivo hemostasis capacity of DBAH was further tested on beating rat and rabbit hearts (Fig. 7d–f). The bleeding of the beating heart was controlled by the DBAH within 1 min with no subsequent bleeding from the wound. Moreover, the DBAH adhesion was sufficiently strong to remain at the bleeding site and was not swept away after 5 min even under dynamic blood pressure flow. Collectively, these results demonstrate that DBAH has excellent in vivo hemostatic performance.

3.8. Effects of DBAH on wound healing

In addition to hemostasis, DBAH can also be used as a wound dressing for wound healing (Fig. 8a). Generally, in comparison with the control group and that treated by PU dressing, wounds managed by DBAH and PEGDA exhibited better healing effects because the hydrogel dressing can absorb wound exudates [35] and prevents wound dehydration while keeping the wound moist to facilitate healing [36]. Moreover, both the macroscopic images and the quantitative data of the wound sections revealed that the DBAH-treated group exhibited quicker healing than the PEGDA group (Fig. 8b–e). Notably, the wound closure rate and granulation tissue thickness in the wound bed were both higher for the DBAH-treated group. Further, a typical proinflammatory factor, interleukin-6 (IL-6), was investigated to evaluate the ability of DBAH in preventing infection. As shown in Fig. 8e, large amounts of IL-6 were detected in the control groups on the ninth day of healing, which suggests a severe inflammatory response owing to a *Staphylococcus aureus* (*S. aureus*) infection. In contrast, little secretion was observed in the DBAH group, indicating minimal inflammation or infection. The efficient wound healing and excellent anti-infection performance of DBAH are attributed likely to its strong integration with the tissue, which enhances cell proliferation and migration and accelerates the growth of new epidermis. Moreover, the close contact of the hydrogel with the surrounding tissue can prevent bacterial infection in the wound during the entire healing period.

4. Conclusion

In summary, we developed a novel dual biomimetic adhesive hydrogel (DBAH) for sealing hemostasis and wound healing with tough wet/dynamic adhesive and excellent antibacterial properties that was inspired by biofilm and the protein secreted by mussels. The robust wet adhesiveness of DBAH is attributed chiefly to the biomimetic polymer CS-MA inspired by the PIA of staphylococcal biofilm. The hydrophobic residues (-CH_3) of the CS-MA rapidly self-repelled water molecules from the adherend interface, thereby resulting in increased exposure of catechol groups of DA and enhancing strong adhesion to the wet tissue surface. The resultant DBAH effectively integrated with the wet tissue contact to seal the wound and rapidly stop the bleeding, even in wet and beating hearts. In addition, this material promoted remarkable healing of a wound infected by *S. aureus* as a full-thickness cutaneous defect while showing biocompatibility. Therefore, DBAH is expected to provide a novel method for in vivo visceral hemostasis and accelerated healing of cutaneous skin wounds.

CRediT authorship contribution statement

Wei Han: Conceptualization, Methodology, Writing - original draft. **Bo Zhou:** Investigation, Data curation. **Kai Yang:** Investigation, Data curation. **Xin Xiong:** Investigation, Data curation. **Shifang Luan:** Resources, Supervision, Validation, Resources, Investigation. **Yu Wang:** Resources, Supervision, Validation. **Zheng Xu:** Resources, Supervision, Validation. **Peng Lei:** Resources, Supervision, Validation. **Zhengshan Luo:** Resources, Supervision, Validation. **Jian Gao:** Resources, Supervision, Validation. **Yijing Zhan:** Resources, Supervision, Validation. **Guopu Chen:** Resources, Supervision, Validation. **Lei Liang:** Resources, Supervision, Validation. **Rui Wang:** Writing - review & editing. **Sha Li:** Writing - review & editing. **Hong Xu:** Writing - review & editing.

Declaration of competing interest

There are no conflict of interest for our manuscript.

Acknowledgements

This work was supported by the National Key R&D Program of China (2019YFA0905203), National Natural Science Foundation of China (51703095), Natural Science Foundation of Jiangsu Province (BK20171010), the State Key Laboratory of Materials- Oriented Chemical Engineering (ZK201905), the Jiangsu Synergetic Innovation Center for Advanced Bio-Manufacture (XTB1804), Jiangsu Agricultural Science and Technology Innovation Fund (CX(19)3115) and the China Postdoctoral Science Foundation (2019M661814).

Appendix A. Supplementary data

Supplementary data to this article can be found online at https://doi.org/10.1016/j.bioactmat.2020.05.008.

References

[1] Y. Hong, F. Zhou, Y. Hua, X. Zhang, C. Ni, D. Pan, Y. Zhang, D. Jiang, L. Yang, Q. Lin, Y. Zou, D. Yu, D.E. Arnot, X. Zou, L. Zhu, S. Zhang, H. Ouyang, Nat. Commun. 10 (2019) 1.
[2] R. Pfeifer, I.S. Tarkin, B. Rocos, H.-C. Pape, Injury 40 (2009) 907.
[3] X. Zhao, B. Guo, H. Wu, Y. Liang, P.X. Ma, Nat. Commun. 9 (2018) 1.
[4] D. Gan, T. Xu, W. Xing, X. Ge, L. Fang, K. Wang, F. Ren, X. Lu, Adv. Funct. Mater. 29 (2019) 1805964.
[5] U. Katzenell, N. Ash, A.L. Tapia, G.A. Campino, E. Glassberg, Mil. Med. 177 (2012) 1065.
[6] C. Cui, C. Fan, Y. Wu, M. Xiao, T. Wu, D. Zhang, X. Chen, B. Liu, Z. Xu, B. Qu, W. Liu, Adv. Mater. 31 (2019) 1905761.
[7] Y. Bu, L. Zhang, G. Sun, F. Sun, J. Liu, F. Yang, P. Tang, D. Wu, Adv. Mater. 31 (2019) 1901580.
[8] X. Zhao, H. Wu, B. Guo, R. Dong, Y. Qiu, P.X. Ma, Biomaterials 122 (2017) 34.
[9] R. Wang, J. Li, W. Chen, T. Xu, S. Yun, Z. Xu, Z. Xu, T. Sato, B. Chi, H. Xu, Adv. Funct. Mater. 27 (2017) 1604894.
[10] Y.S. Zhang, A. Khademhosseini, Science 356 (2017) eaaf3627.
[11] M. Wang, C. Wang, M. Chen, Y. Xi, W. Cheng, C. Mao, T. Xu, X. Zhang, C. Lin, W. Gao, ACS Nano 13 (2019) 10279.
[12] N. Annabi, Y.-N. Zhang, A. Assmann, E.S. Sani, G. Cheng, A.D. Lassaletta, A. Vegh, B. Dehghani, G.U. Ruiz-Esparza, X. Wang, Sci. Transl. Med. 9 (2017) eaai7466.
[13] L. Han, M. Wang, L.O. Prieto-López, X. Deng, J. Cui, Adv. Funct. Mater. (2019) 1907064.
[14] Y. Ahn, Y. Jang, N. Selvapalam, G. Yun, K. Kim, Angew. Chem. Int. Ed. 52 (2013) 3140.
[15] M.V. Rapp, G.P. Maier, H.A. Dobbs, N.J. Higdon, J.H. Waite, A. Butler, J.N. Israelachvili, J. Am. Chem. Soc. 138 (2016) 9013.
[16] K. Kamino, M. Nakano, S. Kanai, FEBS J. 279 (2012) 1750.
[17] D. Gan, W. Xing, L. Jiang, J. Fang, C. Zhao, F. Ren, L. Fang, K. Wang, X. Lu, Nat. Commun. 10 (2019) 1.
[18] L. Han, L. Yan, K. Wang, L. Fang, H. Zhang, Y. Tang, Y. Ding, L. Weng, J. Xu, J. Weng, Y. Liu, F. Ren, X. Lu, NPG Asia Mater. 9 (2017) e372.
[19] Y. Yang, P. Gao, J. Wang, Q. Tu, L. Bai, K. Xiong, H. Qiu, X. Zhao, M.F. Maitz, H. Wang, X. Li, Q. Zhao, Y. Xiao, N. Huang, Z. Yang, Research 10 (2020) 34133.
[20] B.P. Lee, P.B. Messersmith, J.N. Israelachvili, J.H. Waite, Annu. Rev. Mater. Res. 41 (2011) 99.
[21] J.H. Waite, J. Exp. Biol. 220 (2017) 517.
[22] S.K. Clancy, A. Sodano, D.J. Cunningham, S.S. Huang, P.J. Zalicki, S. Shin, B.K. Ahn, Biomacromolecules 17 (2016) 1869.
[23] J. Li, A. Celiz, J. Yang, Q. Yang, I. Wamala, W. Whyte, B. Seo, N. Vasilyev, J. Vlassak, Z. Suo, Science 357 (2017) 378.
[24] H. Yuk, C.E. Varela, C.S. Nabzdyk, X. Mao, R.F. Padera, E.T. Roche, X. Zhao, Nature 575 (2019) 169.
[25] C. Berne, C.K. Ellison, A. Ducret, Y.V. Brun, Nat. Rev. Microbiol. 16 (2018) 616.
[26] C.R. Arciola, D. Campoccia, L. Montanaro, Nat. Rev. Microbiol. 16 (2018) 397.
[27] P.H. Tsang, G. Li, Y.V. Brun, L.B. Freund, J.X. Tang, Proc. Natl. Acad. Sci. Unit. States Am. 103 (2006) 5764.
[28] C.c. Berne, X. Ma, N.A. Licata, B.R. Neves, S. Setayeshgar, Y.V. Brun, B. Dragnea, J. Phys. Chem. B 117 (2013) 10492.
[29] M. Hernando-Pérez, S. Setayeshgar, Y. Hou, R. Temam, Y.V. Brun, B. Dragnea, C. Berne, mBio 9 (2018) e02359.
[30] C.c. Formosa-Dague, C.c. Feuillie, A. Beaussart, S. Derclaye, S.a. Kucharíková, I.i. Lasa, P. Van Dijck, Y.F. Dufrêne, ACS Nano 10 (2016) 3443.
[31] M. Ganesan, E.J. Stewart, J. Szafranski, A.E. Satorius, J.G. Younger, M.J. Solomon, Biomacromolecules 14 (2013) 1474.
[32] B. Li, L. Wang, F. Xu, X. Gang, U. Demirci, D. Wei, Y. Li, Y. Feng, D. Jia, Y. Zhou, Acta Biomater. 22 (2015) 59.
[33] Z. Fan, B. Liu, J. Wang, S. Zhang, Q. Lin, P. Gong, L. Ma, S. Yang, Adv. Funct. Mater. 24 (2014) 3933.
[34] P.K. Campbell, S.L. Bennett, A. Driscoll, A.S. Sawhney, In-vitro Testing, (2005) *1170576081*.1559295193.
[35] C. Ghobril, M. Grinstaff, Chem. Soc. Rev. 44 (2015) 1820.
[36] K. Azuma, M. Nishihara, H. Shimizu, Y. Itoh, O. Takashima, T. Osaki, N. Itoh, T. Imagawa, Y. Murahata, T. Tsuka, Biomaterials 42 (2015) 20.